Published in final edited form as:
*J Phys Chem C Nanomater Interfaces*. 2013 August 8; 117(31): . doi:10.1021/jp406909b.

# Mechanisms of Gadographene-Mediated Proton Spin Relaxation

**Andy H. Hung**[§,†], **Matthew C. Duch**[§,‡], **Giacomo Parigi**[□], **Matthew W. Rotz**[†], **Lisa M. Manus**[†], **Daniel J. Mastarone**[†], **Kevin T. Dam**[†], **Colton C. Gits**[‡], **Keith W. MacRenaris**[†], **Claudio Luchinat**[□], **Mark C. Hersam**[*,‡], and **Thomas J. Meade**[*,†]

[†]Department of Chemistry, Molecular Biosciences, Neurobiology, Biomedical Engineering, and Radiology, Northwestern University, 2145 Sheridan Road, Evanston, Illinois 60208-3113, United States

[‡]Department of Materials Science and Engineering and Department of Chemistry, Northwestern University, 2220 Campus Drive, Evanston, Illinois 60208-3108, United States

[□]CERM and Department of Chemistry, University of Florence, via L. Sacconi 6, 50019 Sesto Florence, Italy

## Abstract

Gd(III) associated with carbon nanomaterials relaxes water proton spins at an effectiveness that approaches or exceeds the theoretical limit for a single bound water molecule. These Gd(III)-labeled materials represent a potential breakthrough in sensitivity for Gd(III)-based contrast agents used for magnetic resonance imaging (MRI). However, their mechanism of action remains unclear. A gadographene library encompassing $GdCl_3$, two different Gd(III)-complexes, graphene oxide (GO), and graphene suspended by two different surfactants and subjected to varying degrees of sonication was prepared and characterized for their relaxometric properties. Gadographene was found to perform comparably to other Gd(III)-carbon nanomaterials; its longitudinal ($r_1$) and transverse ($r_2$) relaxivity is modulated between 12–85 $mM^{-1}s^{-1}$ and 24–115 $mM^{-1}s^{-1}$, respectively, depending on the Gd(III)-carbon backbone combination. The unusually large relaxivity and its variance can be understood under the modified Florence model incorporating the Lipari-Szabo approach. Changes in hydration number ($q$), water residence time ($\tau_M$), molecular tumbling rate ($\tau_R$), and local motion ($\tau_{fast}$) sufficiently explain most of the measured relaxivities. Furthermore, results implicated the coupling between graphene and Gd(III) as a minor contributor to proton spin relaxation.

### Keywords

gadolinium; graphene; graphene oxide; relaxivity; modified Florence NMRD program

**Corresponding Authors**: tmeade@northwestern.edu, m-hersam@northwestern.edu.

[§]**Author Contributions**

These authors contributed equally

**Supporting Information**

Preparation of all gadographene materials, detailed descriptions of the characterization methods, a comprehensive list of all samples studied, validation of $^{17}O$ NMR and [Gd] measurements, full tables of fitted NMRD parameters, theoretical simulations of relaxivities, AFM size histograms, data from dissociation constant experiments, and additional NMRD analyses and discussions are provided. This material is available free of charge via the Internet at http://pubs.acs.org.

The authors declare no competing financial interest.

## Introduction

The effectiveness of Gd(III)-carbon nanomaterials[1–16] in mediating water proton spin relaxation is rarely matched by other Gd(III)-nanomaterial constructs.[17,18] Whether the carbon scaffold has unique properties that contribute to the relaxation process is not yet fully understood. Accelerating proton relaxation underlies the function of contrast agents used in magnetic resonance imaging (MRI).[19–36] Thus, a better elucidation of the mechanism of action of Gd(III)-carbon nanomaterials may provide an opportunity to increase the sensitivity of Gd(III) agents beyond what is currently accessible by Gd(III)-complexes.

Gd(III) relaxes proton spins by creating a fluctuating magnetic field via electronic spin relaxation ($T_{1e}$ and $T_{2e}$) and molecular motion as described by the Solomon-Bloembergen-Morgan (SBM) theory[37–39] and several more advanced theories that account for static zero field splitting (ZFS), namely the slow motion theory,[40–42] the Grenoble approach,[43,44] the Florence model,[45] and the modified Florence model.[46,47] The effectiveness of this process is measured by the relaxation enhancement induced per unit Gd(III) concentration in a quantity known as relaxivity ($mM^{-1}s^{-1}$). The relaxivity of Gd(III)-complexes at 20–60 MHz is typically 4 $mM^{-1}s^{-1}$ and increases to 10–40 $mM^{-1}s^{-1}$ when the complex is conjugated to a slow-tumbling nanomaterial or macromolecule, with the majority of the examples falling between 10–20 $mM^{-1}s^{-1}$.[17,18,37,38,48–54] Exceptional cases include agents that utilize human serum albumin,[55] apoferritin,[56] gold nanoparticle,[57] and viral capsid[58] with reported relaxivities of up to 84 (20 MHz), 80 (20 MHz), 60 (30 MHz), and 202 $mM^{-1}s^{-1}$ (61 MHz), respectively. Gd(III)-carbon nanomaterials such as gadofullerenes,[7,10,12–16] gadonanotubes,[2,6,8,9] and Gd(III)-nanodiamonds[1] studied over the past decade rank among the most potent relaxation agents reported to date. As a class, these materials have achieved relaxivities of up to 50–170 $mM^{-1}s^{-1}$, approaching or even exceeding the theoretical limit for a single water molecule bound to a Gd(III) ion (Figure S1).[37,59]

The impressive relaxivities of Gd(III)-carbon nanomaterials raise speculation regarding the potential role of carbon in mediating unique mechanisms that contribute to proton relaxation.[4,8,12] The theoretical limit for Gd(III) relaxivity is approximately 45 $mM^{-1}s^{-1}$ and 120 $mM^{-1}s^{-1}$ at 60 MHz and 20 MHz, respectively, when assuming isolated paramagnetic centers, single water coordination per metal ($q = 1$), and negligible contribution from second- and outer-sphere waters (Figure S1).[37,59] Of the literature examples that approach or exceed these limits, the viral capsid agent likely has a $q$ larger than 1, the albumin and the gold nanoparticle agents are known to have a $q$ of 2, and the apoferritin agent has large second- and outer-sphere relaxivity. Whether the extraordinary relaxivities of Gd(III)-carbon nanomaterials can be similarly explained is not completely clear due to difficulties in their characterization and structural control. Suggestions have been made that unusual magnetic properties at least partially contribute to the observed relaxivities in some cases.[2,4,8,12] If true, the unique ability of carbon nanomaterials in modulating magnetism would sharply differentiate them from other scaffold materials and present an opportunity to engineer the sensitivity of Gd(III) contrast agents beyond what is currently possible.

The different Gd(III)-carbon nanomaterials are understood to varying degrees with respect to their mechanism of spin relaxation induction. For endohedral gadofullerenes ($r_1$ up to 98 $mM^{-1}s^{-1}$ at 60 MHz),[60] the relaxivity is recognized to derive largely from the exchangeable protons on the fullerene surface and the interstitial water confined between gadofullerenes in an aggregate.[60,61] However, the carbon cage is thought to possess a ½ spin that contributes to relaxivity due to transfer of the $5d^1$ and $6s^2$ electrons from the entrapped Gd(III).[62] For Gd(III)-nanodiamonds ($r_1$ = 59 $mM^{-1}s^{-1}$ at 60 MHz),[1] the mechanism of action is unknown. Potential explanations include slow tumbling rate, nanodiamond clustering, a unique nanoscopic hydration layer,[1] and the two water coordination sites on the Gd(III)-complex.

For carbon nanotubes non-covalently functionalized with amphiphilic Gd(III)-complexes ($r_1$ up to 50 $mM^{-1}s^{-1}$ at 20 MHz), the magnetic susceptibility of the carbon nanomaterial was speculated to contribute to proton relaxation,[8] but no mechanistic study has been performed. For gadonanotubes ($r_1$ = 170 $mM^{-1}s^{-1}$ at 60 MHz)[2] utilizing $GdCl_3$, confinement of the Gd(III) ions has been suggested to induce a superparamagnetic state that enhances the relaxivity of this material.[2] Similar phenomenon seems to have been recapitulated in HiPco single-walled carbon nanotubes[4] and graphene materials with trace Mn(II) ($r_1$ up to 63 $mM^{-1}s^{-1}$ at 20 MHz).[63] However, direct evidence that establishes a causative link between the superparamagnetism and relaxivity has not yet been reported. The question as to whether the carbon scaffold plays a significant role in the unusual relaxivities of Gd(III)-carbon nanomaterials remains unclear.

To better understand the basis of high relaxivity in Gd(III)-carbon nanomaterials, a gadographene library was prepared and studied (Figure 1, Table S1). Graphene is considered to be the parent material of carbon fullerenes and carbon nanotubes; its electronic structure is easily modulated by oxidation[64] and sonication,[65] making it an ideal system of investigation. By systematically changing the carbon backbone, the potential role of the itinerant electrons[66,67] in modulating relaxivity can be clarified. In addition, the different carbon backbones were functionalized with either $GdCl_3$, Gd(III)-DTPA-$NH_2$ ($q$=1), or Gd(III)-DO3A-$NH_2$ ($q$=2). This assortment of materials allowed probing of the contribution from second- and outer-sphere waters and the significance of the mode of association between Gd(III) and the carbon nanomaterial. The gadographenes were carefully checked for metal impurities by ICP-MS (Table S1) and their relaxivities were measured at varying field strengths in Nuclear Magnetic Relaxation Dispersion (NMRD) experiments. For one of the gadographenes, direct measurement of $q$ and magnetic susceptibility ($\chi$) was possible on Gd(III) in its solution state at room temperature, marking the first time these important mechanistic parameters were directly obtained for a Gd(III)-carbon nanomaterial in solution.

## Materials and Methods

### Preparation of Graphene, GO, and reduced GO

The preparation of Graphene, GO, and reduced GO follows previously published methods[68–71] and is described in more detail in Supporting Information. Briefly, sodium cholate (SC)-dispersed graphene was prepared by ultrasonication of graphite (3061 grade, Asbury Graphite Mills) at 40 – 70 W for 45 min – 16 h and purified by removal of large particles via centrifugation (~4,620 g for 30 min), followed by repeated washing and centrifugation in DI water. GO was prepared using a modified Hummer's method,[70] which calls for the treatment of graphite by sulfuric acid and $KMnO_4$, followed by the addition of DI water and 30% $H_2O_2$. The resulting GO was washed by 1:10 HCl solution and DI water on a vacuum filter, ultrasonicated at ~10 W for 1 h, and separated from large aggregates by centrifugation (~21,000 g for 10 min). Reduced GO was prepared by treating dispersed GO solution with 1.5M NaOH for 6 hours under bath sonication,[71] followed by repeated washing and centrifugation in DI water, 1 h ultrasonication at ~10 W, and further centrifugation to remove large particles. Studies by Rourke et al.[72] and Fernandez-Merino, et al.[73] show that the treatment of GO by strong base strips the GO of oxidative debris to achieve a partially reduced, conductive material.

### Preparation of Gadographenes

Functionalization of graphene and GO by $GdCl_3$ follows a previously reported method for gadonanotubes.[2] Briefly, 8 mL of 1 mg/mL $GdCl_3$ solution was mixed with 8 mg of graphene or GO and bath sonicated for 1 h. The sample was left undisturbed for 12 h, and then washed by repeated centrifugation and re-suspension in DI water. The resulting

material was dispersed in either 2%SC/2%PL solution or DI water by ultrasonication for 1 h at ~10 W. Large aggregates were removed by centrifugation to complete the processing. Functionalization of graphene and GO by Gd(III)-complexes (Gd(III)-DO3A-$NH_2$ or Gd(III)-DTPA-$NH_2$) was performed by using 1-Ethyl-3-(3-dimethylaminopropyl)carbodiimide[1] and basic pH,[74–77] respectively. Details of the Gd(III)-complex syntheses and reaction conditions are available in Supporting Information. Excess Gd(III)-complexes and activating agents were removed by repeated washing and centrifugation. The same functionalization procedures were followed for both GO and reduced GO.

### NMRD and 60 MHz Relaxivity Measurments

The $T_1$ of water protons at 0.01–40 MHz Larmor frequency was measured by a Stelar Spinmaster FFC-2000-1T fast field cycling relaxometer. A Bruker mq60 minispec relaxometer was used to measure the relaxivity at 60 MHz. $T_1$ measurements were performed by an inversion recovery pulse sequence. $T_2$ measurements were performed by a Carr-Purcell-Meiboom-Gill pulse sequence with 1 ms 90°–180° pulse separation. Relaxivity was obtained by linear fitting $1/T_{1,2}$ against Gd(III) concentration. Measurement on graphene, GO, 2%SC, and 2%PL controls, and methods used to correct for contributions from impurities are detailed in Supporting Information.

### Gd(III) Concentration Determination

Gd(III) concentration was measured by Inductively Coupled Plasmon-Mass Spectrometry (ICP-MS) and cross-validated by ICP-Optical Emission Spectroscopy (ICP-OES) across two sample digestion protocols (Table S7). Sample digestion was performed by incubation with ≥ 69% $HNO_3$ at 60°C overnight, or alternatively by substituting $HNO_3$ with 3:2 $HNO_3$:$H_2O_2$ (30% w/w). Iron impurity concentration was measured in addition to Gd(III) concentration. Other metal impurities were characterized by the ICP-MS survey scan, but not measured quantitatively.

## Results and Discussion

The gadographene library consists of seven different materials (Figure 1, Table S1). Each of graphene oxide (GO), graphene in 2% F108NF pluronic acid (PL), or graphene in 2% sodium cholate (SC) was functionalized with either $GdCl_3$ or Gd(III)-DO3A-$NH_2$; additionally, a GO with Gd(III)-DTPA-$NH_2$ was prepared. Whether the Gd(III)-complexes are covalently linked or simply adsorbed to the carbon nanomaterial is unclear, but the uncertainty does not detract from the interpretation of the results. The relaxivity (measured at 60 MHz) of gadographene is modulated by sonication and the choice of Gd(III)-carbon combination. In some cases, gadographene recapitulates the high relaxivity of other Gd(III)-carbon nanomaterials, validating its relevance as a system for mechanistic investigation.

### Relaxivity Trends

Several relaxivity trends (Figure 2) in gadographene suggest a possibly unique role of the carbon scaffold in modulating relaxivity. The first indication is the opposing trends between Gd(III) Graphene 2%PL and Gd(III) Graphene 2%SC as sonication increases (Figure 2A). According to SBM equations (see Supporting Information), relaxivity at 60 MHz *decreases* with smaller scaffolds and faster molecular tumbling (small $\tau_R$) under the typical scenario of $\tau_R < 5$ ns and $T_{1e} >> \tau_R$ (Figure S1). Since graphene flake size tends to decrease with sonication, the decreasing trend in the 2%PL samples is consistent with theory. However, the same explanation does not apply to the increasing trend in the 2%SC samples. To rationalize this result, the special case of $\tau_R$, $\tau_M > 10$ ns may be considered ($\tau_M$ is the water residence time). In this regime, the theoretical $r_1$ at 60 MHz *increases* with smaller flake size

to match the experimental measurements (Figure S2). However, while this hypothetical scenario explains the observed $r_1$ trend, it fails to account for the increasing $r_2$ trend. Therefore, the trending of relaxivity with sonication is not consistent with an interpretation using flake size. Further confirmation was obtained when experiments showed an absence of pronounced correlation between relaxivity and graphene size as measured by both Dynamic Light Scattering (DLS) and Atomic Force Microscopy (AFM) (Figure 2B, Figure S3). Hence, contrary to expectation, there is little evidence to support molecular tumbling as the primary explanatory factor for the correlation between relaxivity and sonication.

Alternatively, it is possible that the relative portion of Gd(III) distributed to the graphene planes increases with sonication as compared to the portion distributed to the edges. With one exception (Gd(III) Graphene 2%SC 30 W-hr), the DLS data shows that graphene size decreases with sonication (Figure 2B). The origin of this decrease is likely due to a decrease in thickness (Figure 2B) as no correlation was observed between graphene area and sonication (Figure S3). When sonication is increased, relatively more Gd(III) would be distributed to the planes as a result of the thinner graphene stacks. If the relaxivity of the planar Gd(III) population is larger than that of the edge population in the 2%SC samples (and vice versa in the 2%PL samples), then the observed relaxivity trends can be explained.

A further explanation may be that graphene damage modulates relaxivity in a surfactant-dependent manner. Damage in the form of sonication-induced defects and oxidation can alter the $\tau_M$ or the effective correlation time ($\tau_c^{-1} = \tau_R^{-1} + \tau_M^{-1} + T_{1e}^{-1}$) of gadographene, or modulate the electronic, and in turn, the magnetic properties of the material.[67] Intriguingly, trends in the transverse-to-longitudinal relaxivity ratio ($r_2/r_1$) correlate with damage (Figure 2A, C). Gd(III) Graphenes possess $r_2/r_1$ ratios that exceed 1.2, suggesting that their $\tau_c$ and $\tau_M$ are longer than 1 ns (Figure S2). One interpretation is that as damage increased, the $r_2/r_1$ correspondingly decreased to imply a decline in $\tau_c$ or $\tau_M$. However, this interpretation may be flawed for Gd(III) Graphene 2%SC because the material's decreasing trend in $r_2/r_1$ cannot be reconciled with its increasing trend in $r_1$ and $r_2$ under *any* combination of $\tau_R$ and $\tau_M$ (Figure S2). Consequently, a different interpretation of the $r_2/r_1$ data is desirable.

Large $r_2/r_1$ that exceed those typically reported for paramagnetic ions is a notable property of gadonanotubes[2,11] and graphene with Mn(II) impurities[63] (3–9 compared to ~ 1 for Gd(III)-complexes). Both of these materials possess unusual $r_1$ NMRD profiles beyond the explanatory power of SBM theory. While the $r_2/r_1$ of gadographenes are not as pronounced, samples utilizing more pristine graphene had consistently larger ratios when compared to more sonicated graphene and GO, regardless of whether $GdCl_3$ or Gd(III)-complexes were used (Figure 2A, C). By drawing analogy to other Gd(III)-carbon nanomaterials, these trends in $r_2/r_1$ suggest the possibility that graphene damage may influence relaxivity through contributions unaccounted for by current theory. If the effect of graphene damage interacts with surfactant choice, then the opposite effect of sonication on Gd(III) Graphene 2%SC and Gd(III) Graphene 2%PL can be understood.

Given the empirical trends that circumstantially implicate graphene as a unique modulator of relaxivity, magnetic properties that can originate from the graphene itinerant electrons[66,67] were examined more closely. Materials based on non-conductive GO[64] were compared to materials based on graphene. For both $GdCl_3$ and Gd(III)-complexes, higher relaxivity was achieved using GO, indicating that the presence of itinerant electrons is not crucial for gadographene relaxivity (Figure 1, S4). Further investigation of the potential magnetic coupling between Gd(III) and the carbon backbone was performed by comparing gadographene to analogs that use other metals of large magnetic moment, namely iron and terbium. The relaxivities of these analogs decreased by more than 10 fold when compared to

gadographene (Figure S4), suggesting that any magnetic coupling between Gd(III) and graphitic carbon does not generalize to other metal ions even if it were present. These results imply that magnetism or other intrinsic mechanisms in graphene are not the determinant of gadographene relaxivity, although they may play a secondary role.

Similar to the ideas proposed for other Gd(III)-carbon nanomaterials, suggestive evidence was found implicating graphene as a unique modulator of relaxivity. At the same time, the results indicate that the contribution is at most minor, leaving the mechanism for the unusually large relaxivities of gadographene up for further elucidation. Additionally, the basis of the difference in relaxivity among agents utilizing GO, 2% PL graphene, and 2% SC graphene, and the reason for Gd(III)-DO3A GO to have a comparable relaxivity to Gd(III) GO despite a lower expected $q$ (Figure 1) pose further questions. To gain a more detailed mechanistic understanding of gadographene relaxivity, NMRDs were acquired and analyzed by the modified Florence program (SI Materials and Methods).[26,27] This more advanced model was used for NMRD analysis because SBM theory does not take into account static ZFS that determines the spin energy levels at low fields (< 10 MHz). At high fields, Zeeman interactions dominate, and the two theories converge.

### Gd(III) Graphene Oxide

Within the gadographene library, Gd(III) GO is the most well characterized and understood. Its high Gd(III) loading allowed for preparation of samples with sub-millimolar Gd concentration to enable the measurement of $q$ and $\chi$ by $^{17}O$ NMR.[78] These mechanistic parameters have never been directly measured for a Gd(III)-carbon nanomaterial due to incompatibility with conventional methods. Typically, the fluorescence lifetime of Eu(III) or Tb(III) analogs of a Gd(III)-complex is used to measure its $q$.[79] However, whether $q$ is conserved across analogs beyond well-defined coordination complexes is unknown. Furthermore, carbon nanomaterials often quench fluorescence[80] and are difficult to prepare at sufficiently high concentrations for the measurement. For $\chi$, a Semiconducting Quantum Interference Device (SQUID) is usually employed, but the samples must be in solid state. Here, by observing the $^{17}O$ chemical shift with and without field locking against a GO control by NMR, the $q$ and $\chi$ of Gd(III) GO is directly measured in solution at 296 K and 353 K. The $q$ measured was 5 (Figure 3, Table S2), consistent with the measured dissociation constant of $10^{-8}$ – $10^{-10}$ M to indicate weakly coordinated Gd(III) ions (Figure S5). The effective magnetic moment ($\mu_{eff}$) measured was 7.3 (Figure 3, Table S2), compared to the theoretical value of 7.9[81] to imply a $\chi$ that is consistent with paramagnetic Gd(III) ions. In other words, no unusual magnetic properties were observed with Gd(III) GO.

To further understand the relaxivity of Gd(III) GO, its $\tau_M$ and $\tau_R$ were characterized. For $\tau_M$, there is no established method available for direct measurement on Gd(III) agents that are slow-tumbling ($\tau_R$ > 1 ns). Nevertheless, $\tau_M$ was determined to be in the fast-exchange regime (≤ 10 ns) by comparing NMRD measurements at two temperatures. Water exchange is defined to be fast or slow in relation to the relaxation time of the water protons dipole-dipole coupled to Gd(III).[82] When $\tau_M$ is in the slow-exchange regime, the faster molecular motion and water exchange at higher temperature have opposite effects on relaxivity. The two effects can cancel to result in a weak temperature-dependence of the NMRD profiles, but more often, the outcome is an increase of $r_1$ with increasing temperature due to the dominant effect of water exchange. When $\tau_M$ is in the fast-exchange regime, $\tau_R$ is the main limiting factor, and higher temperature results in lower relaxivities due to faster molecular tumbling. Based on these expectations, the data for Gd(III) GO indicates that its $\tau_M$ is in the fast-exchange regime (Figure 3). To further confirm this result, quantitative fits of the NMRD profiles were obtained. The fitted $\tau_M$ values were 0.74 ns and 0.64 ns at 298 K and 310 K, respectively (Figure 3), approximating the $\tau_M$ of Gd(III) aqua ions (0.94 ns at 310 K)[37] and consistent with the expected temperature dependence.

For $\tau_R$, HYDRONMR[83] simulation of a graphene model was used to provide guidance in selecting a range of reasonable values. Result showed the expected $\tau_R$ to be greater than 1000 ns for a perfectly rigid graphene flake of the dimensions used in this study (SI Materials and Methods). In this range, $\tau_R$ does not affect NMRD fitting, and therefore was fixed in our analysis. However, using the modified Florence program, the fitted profiles exhibited high field (> 10 MHz) peaks that were too broad for the collected data points (Figure 3A). This feature persisted even when best-fits based on smaller $\tau_R$ were forced (unpublished results). When the Lipari-Szabo approach[84] was incorporated into the modified Florence model[85] as an alternative, the fits improved markedly (Figure 3B).

The Lipari-Szabo formalism treats a system as having two correlation times ($\tau_{fast}$ and $\tau_R$) related to two completely uncoupled motions without assuming their precise nature. The order parameter $S^2$ models the degree of spatial restriction of the fast motion, with 0 being no restriction and 1 being complete restriction. For Gd(III) GO, the two correlation times do not correspond to anisotropic tumbling. When a graphene stack of $3.6 \times 150 \times 150$ Å$^3$ was modeled by HYDRONMR, all five components of the rotational diffusion tensor were calculated to be greater than 100 ns despite the model being ten times smaller than the experimental samples studied. This prediction is inconsistent with the fitted $\tau_{fast}$ that fell below 0.5 ns regardless of the $\tau_R$ chosen, indicating that the captured NMRD feature is not related to anisotropy. Therefore, $\tau_{fast}$ most likely reflects fast local motions related to either the mobility of the Gd(III) ions with respect to the carbon scaffold,[86] the swapping of coordinated waters, or the pseudorotation rearrangement of the Gd(III) hydration shell.[87] These fast motions cause incomplete reorientation of the proton–Gd(III) vector in timescales faster than the overall tumbling time of the system.

Results of fitting after incorporation of the Lipari-Szabo approach showed $\tau_{fast}$ to be approximately 100 ps with a $S^2$ of 0.43. This timescale is similar to that of free-tumbling small molecule Gd(III)-complexes. As expected, the adjusted $\tau_M$ (1.6 ns at 310 K) remained close to that of Gd(III) aqua ions. For secondary validation, the best-fit parameters were used to calculate the theoretical $r_2$. The measured and predicted values agreed with each other, confirming that the obtained parameters are indeed reasonable (Figure 3).

In summary, the high relaxivity of Gd(III) GO results from the combination of $q = 5$ and large $\tau_R$, and is limited by short water residence time and fast local motion. Based on HYDRONMR simulation, GO may be an attractive scaffold for high relaxivity Gd(III) agents because its sheet geometry results in a $\tau_R$ that is larger than what a spherical scaffold of the same mass would exhibit. No evidence suggested any unusual magnetic behavior. The NMRD of Gd(III) GO can be completely interpreted within the available theory.

## Gd(III) Graphene

To further elucidate whether the relaxivity of gadographene is influenced by the carbon scaffold beyond its $\tau_R$ properties, materials utilizing different graphene backbones were investigated. Specifically, Gd(III) GO, Gd(III) Graphene 2%SC, and Gd(III) Graphene 2%PL were compared, and materials receiving different doses of sonication were analyzed. Results showed that most of the relaxivity variations can be explained by the modified Florence model, but not all. The small, unexplained portion of the variation should not be overlooked because it points to processes related to pristine graphene that can potentially be engineered to further enhance relaxivity. Unlike Gd(III) GO, Gd(III) Graphenes were not amenable to $^{17}$O NMR studies due to their lower Gd(III) loading. Consequently, findings from Gd(III) GO were relied upon as anchoring points for data interpretation. The comparable Gd(III) dissociation constants of the three agents suggest that this approach is reasonable (Figure S5). Similar to Gd(III) GO, NMRD profiles of Gd(III) graphene consistently found better fits with the Lipari-Szabo approach than without, indicating the

likely existence of fast local motions (Figure S6). Beyond this conclusion, it was only possible to interpret the data by several equally plausible scenarios because solutions from NMRD fitting are not unique without independent measurements of the fitting parameters $q$ and $\tau_M$.

The different relaxivities of Gd(III) GO, Gd(III) Graphene 2%SC, and Gd(III) Graphene 2%PL at 60 MHz may be accounted for by one of three possible explanations: 1) $q$, 2) $\tau_{fast}$ and $S^2$, or 3) $\tau_M$. For $q$, the three agents may differ as a result of the suspending surfactants. Due to the carboxyl group on SC and the polymeric nature of PL (Figure S7), it is conceivable that transient interactions could change the effective $q$ of Gd(III) when the surfactants are used at 2% w/v concentrations. Quantitative analysis showed that the idea is plausible (Figure 4A). When $\tau_R$, $\tau_{fast}$, and $\tau_M$ were fixed to the values obtained for Gd(III) GO, satisfactory NMRD fits were obtained for the GO, SC, and PL samples at a $q$ of 5, 3, and 2, respectively; additionally, a small difference in $S^2$ was noted between the GO and the graphene samples.

Alternatively, the observed relaxivity differences could be attributed to the dissimilar local Gd(III) environments in the GO, SC, and PL samples. Although the details are difficult to pinpoint, the surfactants and the different surface groups on GO and graphene can both contribute to creating unique microenvironments for the Gd(III) ions in each of the three agents. These differences would manifest in the $\tau_{fast}$ and $S^2$ values in NMRD analysis. Global tumbling was ruled out as a factor in controlling Gd(III) Graphene relaxivity because the graphene flakes studied more than doubled the size of the models used in HYDRONMR simulation. Therefore, $\tau_R \geq 1000$ ns was maintained in the NMRD fits. Results showed that $\tau_{fast}$ and $S^2$ are indeed sufficient to explain the relaxivity differences, with the graphene samples exhibiting smaller order parameters and faster local motions than the GO sample (Figure 4B).

Finally, $\tau_M$ provides a third possible explanation for the different relaxivities of Gd(III) GO and SC- and PL-suspended Gd(III) Graphene. Intuitively, surfactants in Gd(III) Graphene reduce relaxivity by posing a diffusion barrier. To test this idea, two-temperature NMRD experiments were performed to probe $\tau_M$ (Figure S8). Unfortunately, while larger relaxivities were observed at the lower temperature, the difference was small. Therefore, it is ambiguous whether $\tau_M$ shifted into the slow-exchange regime as a result of the suspending surfactants in Gd(III) Graphene.

The observed relaxivity differences among Gd(III) GO and Gd(III) Graphenes can be attributed to the individual or combined effects of $q$, $\tau_{fast}$, $S^2$, and $\tau_M$. Regardless of the actual mechanism, all of the proposed possibilities are understandable within the current theoretical framework. NMRD analysis of Gd(III) Graphenes at varying sonication dose suggests that graphene properties additionally contribute to the relaxivity differences observed (Figure S9). First, the unpaired Gd(III) electron $T_{1e}$ at 100 kHz negatively correlates with sonication and is longer in Gd(III) Graphene (~ 300 ps) than in Gd(III) GO (~ 200 ps), suggesting that graphene damage and/or surfactants may be modulating the electronic relaxation process (Figure S9). Second, NMRD further confirmed the previous analysis that the opposite 60 MHz relaxivity trends between the SC- and PL-suspended Gd(III) Graphenes cannot be interpreted by flake size (Figure 2A, Figure S9). Third, unlike for Gd(III) GO, theoretical predictions consistently underestimated the measured $r_2$ for Gd(III) Graphenes (Figure 4, Figure S9). Theory miscalculated by 32% for the most pristine graphene and predicted with increasing accuracy for the more damaged samples, consistent with the noted trends in $r_2/r_1$ ratio. Unusually large scalar interactions or a chemical shift difference between water molecules confined within graphene stacks and the bulk can be speculated to provide an interpretation of the data and are discussed further in

Supplementary Note S1. Trivial explanations related to the residual Fe ions in the samples were ruled out by correcting for their contributions to $r_2$ (SI Materials and Methods). The data suggests that there are hidden parameters (including those related to intrinsic mechanisms of graphene) contributing to the relaxivity of Gd(III) Graphene but not that of Gd(III) GO.

### Gd(III)-Complex Graphene Oxide

Gd(III)-DTPA-$NH_2$ ($q$=1) and Gd(III)-DO3A-$NH_2$ ($q$=2) conjugated to GO and partially reduced GO (rGO)[72,73] are valuable agents in the mechanistic investigation of gadographene relaxivity for two reasons: 1) their $q$ are systematically controlled and 2) their Gd(III) ions couple into the carbon backbone indirectly via a coordinating complex, in contrast to the ionic gadographenes. Beyond their fundamental interest, these agents may be of practical value because the use of complexes makes them potentially compatible with *in vivo* applications.

By comparing gadographenes based on the two different complexes, inferences can be made about the relative contributions of inner- and outer-sphere effects to relaxivity. The relaxivity of the $q$=2 complex (Gd(III)-DO3A-$NH_2$) was found to be almost exactly double that of the $q$=1 complex (Gd(III)-DTPA-$NH_2$) for both GO and rGO (Figure 1). This result implies that gadographene relaxivity derives mostly from inner-sphere effects with only minor contributions from outer-sphere effects, in agreement with the analyses performed for Gd(III) GO and Gd(III) Graphene.

By comparing the complexed version and the ionic version of the same agent, we examined if the mode of association between Gd(III) ions and the carbon backbone influences relaxivity. Magnetic interactions mediated by the carbon itinerant electrons[66,67] could potentially amplify relaxivity, and the mode of association may modulate these interactions. Intriguingly, results showed the relaxivities of Gd(III)-complex GO to be much closer to Gd(III) GO than would be expected given their lower $q$ (Figure 1). In the absence of significant outer-sphere effects, this result indicates that the Gd(III) ions are more efficient at relaxing water protons on a per-coordination-site basis when they are complexed compared to when they are associated directly with the carbon backbone in gadographene.

To better understand the origin of this observation, NMRD profiles of Gd(III)-complex GO were acquired and analyzed (Figure 5). Assuming $\tau_R > 1000$ ns as before and that the $\tau_M$ of the complexes[37] remain unchanged post-conjugation, the high relaxation efficiency of Gd(III)-complex GO can be satisfactorily explained by their optimized correlation times (for local motion, $\tau_{cl}^{-1} = \tau_R^{-1} + \tau_M^{-1} + T_{1e\,-1} + \tau_{fast}^{-1}$)[84,88] without having to evoke unusual magnetic properties. The use of complexes prolonged $\tau_M$ by approximately two orders of magnitude and $\tau_{fast}$ by one order of magnitude compared to Gd(III) ions. As a result, $\tau_{cl}$ increased towards the optimal condition of $\tau_{cl} = 1/\nu_H$ with a concomitant increase in relaxivity ($\nu_H$ is the proton Larmor frequency). Interestingly, although the $\tau_{fast}$ of the agent is about ten times slower than the $\tau_R$ of a free complex, the near-zero $S^2$ of the fits suggest that the complexes experience isotropic tumbling independent of the motions of the GO scaffold. Therefore, in addition to slowing down water exchange and eliminating the type of local motions associated with Gd(III) ions, Gd(III)-complexes evidently undergo slow reorientation on the GO surface and consequently experience an enhancement in relaxivity.

To further examine the effect that the carbon backbone may have on relaxivity beyond contributing slow global motion, the GO and the rGO version of the agent were compared. Consistent with the findings in Gd(III) Graphene, the best-fit parameters obtained from NMRD analysis did not accurately predict the measured $r_2$ (60 MHz) of all agents (Figure 5). Notably, theory underestimated the $r_2$ of Gd(III)-DO3A-$NH_2$ when rGO (but not when

GO) was used as the carbon scaffold. rGO is known to more closely mimic graphene with an increased conductivity when compared to GO.[72,73] These results suggest that pristine graphene contributes weakly to relaxivity, consistent with the observation in comparing Gd(III) Graphene with Gd(III) GO.

In summary, gadographenes utilizing Gd(III)-complexes are more efficient at relaxing the proton spins of each coordinated water compared to analogs utilizing Gd(III) ions. Based on NMRD analysis, the likely reason for this result is that the complexes used have relatively optimal $\tau_M$ and eliminate fast local motions that Gd(III) ions experience; these effects are completely inner-sphere. Although no unusual magnetic properties were required to explain most of the measured relaxivities, the $r_2$ of these materials could not be consistently predicted and implicate graphene-related processes as a weak contributor to relaxivity. Gd(III)-complex GO achieved high relaxivity despite near-zero dependence on the global tumbling of GO. Thus, an opportunity may exist for this class of agents to achieve the maximum theoretical relaxivity if local mobility can be removed.

## Conclusions

Gadographenes are a suitable model system for elucidating the mechanistic origin of high relaxivity exhibited by Gd(III)-carbon nanomaterials. In particular, the question as to whether graphene magnetism contributes to gadographene relaxivity was examined. It was found that the agents can be described using the modified Florence model of relaxation without having to evoke significant unusual magnetic behaviors or second- or outer-sphere effects. Specifically, the high relaxivities of the ionic gadographenes were attributed to $q > 1$ and slow tumbling, while those of the complexed samples were further enhanced per coordinated water due to optimal water exchange and slow local motion. Additionally, several relaxivity trends suggest pristine graphene as a potential weak contributor to gadographene relaxivity and present future opportunities for further investigation and engineering.

## Supplementary Material

Refer to Web version on PubMed Central for supplementary material.

## Acknowledgments

This work was supported by NIH Grant R01EB014806, the National Cancer Institute Center for Cancer Nanotechnology Excellence initiative at Northwestern University Award No. U54CA151880, the Ente Cassa di Risparmio di Firenze, and the European Commission contract Bio-NMR no. 261863, and a Cooperative Agreement between the National Science Foundation and the Environmental Protection Agency (DBI 0830117). The authors thank the Northwestern University Integrated Molecular Structure Education and Research Center (IMSERC); a description of the facility and full funding disclosure can be found at http://asllogins rv.chem.northwestern.edu/analyticalserviceslab/asl.htm.

## References

1. Manus LM, Mastarone DJ, Waters EA, Zhang XQ, Schultz-Sikma EA, MacRenaris KW, Ho D, Meade TJ. Gd(III)-Nanodiamond Conjugates for MRI Contrast Enhancement. Nano Lett. 2010; 10:484–489. [PubMed: 20038088]
2. Sitharaman B, Kissell KR, Hartman KB, Tran LA, Baikalov A, Rusakova I, Sun Y, Khant HA, Ludtke SJ, Chiu W, Laus S, Toth E, Helm L, Merbach AE, Wilson LJ. Superparamagnetic Gadonanotubes Are High-Performance MRI Contrast Agents. Chem. Commun. 2005:3915–3917.
3. Sitharaman B, Wilson LJ. Gadofullerenes and Gadonanotubes: A New Paradigm for High-Performance Magnetic Resonance Imaging Contrast Agent Probes. J. Biomed. Nanotechnol. 2007; 3:342–352.

4. Ananta JS, Matson ML, Tang AM, Mandal T, Lin S, Wong K, Wong ST, Wilson LJ. Single-Walled Carbon Nanotube Materials as T2-Weighted MRI Contrast Agents. J. Phys. Chem. C. 2009; 113:19369–19372.
5. Chan BTY, Hassan AA, Hartman KB, Ananta JS, Mackeyev Y, Hu L, Pautler RG, Wilson LJ, Lee AV. Utilization of Serine-Derivatized Gadonanotubes as Magnetic Nanoprobes for Intracellular Labeling of MCF-7 Human Breast Cancer Cell. Cancer Res. 2009; 69:766s–766s.
6. Hartman KB, Laus S, Bolskar RD, Muthupillai R, Helm L, Toth E, Merbach AE, Wilson LJ. Gadonanotubes as Ultrasensitive pH-Smart Probes for Magnetic Resonance Imaging. Nano Lett. 2008; 8:415–419. [PubMed: 18215084]
7. Kato H, Kanazawa Y, Okumura M, Taninaka A, Yokawa T, Shinohara H. Lanthanoid Endohedral Metallofullerenols for MRI Contrast Agents. J. Am. Chem. Soc. 2003; 125:4391–4397. [PubMed: 12670265]
8. Richard C, Doan BT, Beloeil JC, Bessodes M, Toth E, Scherman D. Noncovalent Functionalization of Carbon Nanotubes with Amphiphilic Gd3+ Chelates: Toward Powerful T1 and T2 MRI Contrast Agents. Nano Lett. 2008; 8:232–236. [PubMed: 18088153]
9. Sethi R, Mackeyev Y, Wilson LJ. The Gadonanotubes Revisited: A New Frontier in MRI Contrast Agent Design. Inorg. Chim. Acta. 2012; 393:165–172.
10. Shu CY, Corwin FD, Zhang JF, Chen ZJ, Reid JE, Sun MH, Xu W, Sim JH, Wang CR, Fatouros PP, Esker AR, Gibson HW, Dorn HC. Facile Preparation of a New Gadofullerene-Based Magnetic Resonance Imaging Contrast Agent with High 1H Relaxivity. Bioconjugate Chem. 2009; 20:1186–1193.
11. Sitharaman B, Van Der Zande M, Ananta JS, Shi XF, Veltien A, Walboomers XF, Wilson LJ, Mikos AG, Heerschap A, Jansen JA. Magnetic Resonance Imaging Studies on Gadonanotube-Reinforced Biodegradable Polymer Nanocomposites. J. Biomed. Mater. Res. A. 2010; 93A:1454–1462. [PubMed: 19927368]
12. Toth E, Bolskar RD, Borel A, Gonzalez G, Helm L, Merbach AE, Sitharaman B, Wilson LJ. Water-Soluble Gadofullerenes: Toward High-Relaxivity, pH-Responsive MRI Contrast Agents. J. Am. Chem. Soc. 2005; 127:799–805. [PubMed: 15643906]
13. Zhang JF, Fatouros PP, Shu CY, Reid J, Owens LS, Cai T, Gibson HW, Long GL, Corwin FD, Chen ZJ, Dorn HC. High Relaxivity Trimetallic Nitride (Gd3n) Metallofullerene MRI Contrast Agents with Optimized Functionality. Bioconjugate Chem. 2010; 21:610–615.
14. Bolskar RD. Gadofullerene MRI Contrast Agents. Nanomedicine. 2008; 3:201–213. [PubMed: 18373426]
15. Mikawa M, Kato H, Okumura M, Narazaki M, Kanazawa Y, Miwa N, Shinohara H. Paramagnetic Water-Soluble Metallofullerenes Having the Highest Relaxivity for MRI Contrast Agents. Bioconjugate Chem. 2001; 12:510–514.
16. Bolskar RD, Benedetto AF, Husebo LO, Price RE, Jackson EF, Wallace S, Wilson LJ, Alford JM. First Soluble M@C60 Derivatives Provide Enhanced Access to Metallofullerenes and Permit in Vivo Evaluation of Gd@C60[C(COOH)(2)](10) as a MRI Contrast Agent. J. Am. Chem. Soc. 2003; 125:5471–5478. [PubMed: 12720461]
17. Botta M, Tei L. Relaxivity Enhancement in Macromolecular and Nanosized Gd(III)-Based MRI Contrast Agents. Eur. J. Inorg. Chem. 2012:1945–1960.
18. Liu YJ, Zhang N. Gadolinium Loaded Nanoparticles in Theranostic Magnetic Resonance Imaging. Biomaterials. 2012; 33:5363–5375. [PubMed: 22521487]
19. Allen MJ, Meade TJ. Synthesis and Visualization of a Membrane-Permeable MRI Contrast Agent. J. Biol. Inorg. Chem. 2003; 8:746–750. [PubMed: 14505078]
20. Manus LM, Strauch RC, Hung AH, Eckermann AL, Meade TJ. Analytical Methods for Characterizing Magnetic Resonance Probes. Anal. Chem. 2012; 84:6278–6287. [PubMed: 22624599]
21. Powell DH, NiDhubhghaill OM, Pubanz D, Helm L, Lebedev YS, Schlaepfer W, Merbach AE. Structural and Dynamic Parameters Obtained from 17O NMR, EPR, and NMRD Studies of Monomeric and Dimeric Gd3+ Complexes of Interest in Magnetic Resonance Imaging: An Integrated and Theoretically Self Consistent Approach. J. Am. Chem. Soc. 1996; 118:9333–9346.

22. Mastarone DJ, Harrison VSR, Eckermann AL, Parigi G, Luchinat C, Meade TJ. A Modular System for the Synthesis of Multiplexed Magnetic Resonance Probes. J. Am. Chem. Soc. 2011; 133:5329–5337. [PubMed: 21413801]
23. Qin J, Laurent S, Jo YS, Roch A, Mikhaylova M, Bhujwalla ZM, Muller RN, Muhammed M. A High-Performance Magnetic Resonance Imaging T2 Contrast Agent. Adv. Mater. 2007; 19:1874–1878.
24. Matosziuk LM, Harney AS, MacRenaris KW, Meade TJ. Synthesis, Characterization, and in Vitro Testing of a Bacteria-Targeted MR Contrast Agent. Eur. J. Inorg. Chem. 2012:2099–2107. [PubMed: 23626484]
25. Sherry AD, Caravan P, Lenkinski RE. Primer on Gadolinium Chemistry. J. Magn. Reson. Imaging. 2009; 30:1240–1248. [PubMed: 19938036]
26. Zhang SR, Wu KC, Sherry AD. A Novel pH-Sensitive MRI Contrast Agent. Angew. Chem. Int. Ed. 1999; 38:3192–3194.
27. Li WH, Fraser SE, Meade TJ. A Calcium-Sensitive Magnetic Resonance Imaging Contrast Agent. J. Am. Chem. Soc. 1999; 121:1413–1414.
28. De Leon-Rodriguez LM, Lubag AJM, Malloy CR, Martinez GV, Gillies RJ, Sherry AD. Responsive MRI Agents for Sensing Metabolism in Vivo. Acc. Chem. Res. 2009; 42:948–957. [PubMed: 19265438]
29. Major JL, Parigi G, Luchinat C, Meade TJ. The Synthesis and in Vitro Testing of a Zinc-Activated MRI Contrast Agent. Proc. Natl. Acad. Sci. U. S. A. 2007; 104:13881–13886. [PubMed: 17724345]
30. Song Y, Kohlmeir EK, Meade TJ. Synthesis of Multimeric MR Contrast Agents for Cellular Imaging. J. Am. Chem. Soc. 2008; 130:6662–6663. [PubMed: 18452288]
31. Louie AY, Huber MM, Ahrens ET, Rothbacher U, Moats R, Jacobs RE, Fraser SE, Meade TJ. In Vivo Visualization of Gene Expression Using Magnetic Resonance Imaging. Nat. Biotechnol. 2000; 18:321–325. [PubMed: 10700150]
32. Roch A, Muller RN, Gillis P. Theory of Proton Relaxation Induced by Superparamagnetic Particles. J. Chem. Phys. 1999; 110:5403–5411.
33. Sukerkar PA, MacRenaris KW, Meade TJ, Burdettes JE. A Steroid- Conjugated Magnetic Resonance Probe Enhances Contrast in Progesterone Receptor Expressing Organs and Tumors in Vivo. Mol. Pharm. 2011; 8:1390–1400. [PubMed: 21736390]
34. Esqueda AC, Lopez JA, Andreu-De-Riquer G, Alvarado-Monzon JC, Ratnakar J, Lubag AJM, Sherry AD, De Leon-Rodriguez LM. A New Gadolinium- Based MRI Zinc Sensor. J. Am. Chem. Soc. 2009; 131:11387–11391. [PubMed: 19630391]
35. Strauch RC, Mastarone DJ, Sukerkar PA, Song Y, Ipsaro JJ, Meade TJ. Reporter Protein-Targeted Probes for Magnetic Resonance Imaging. J. Am. Chem. Soc. 2011; 133:16346–16349. [PubMed: 21942425]
36. Hu FQ, MacRenaris KW, Waters EA, Liang TY, Schultz-Sikma EA, Eckermann AL, Meade TJ. Ultrasmall, Water-Soluble Magnetite Nanoparticles with High Relaxivity for Magnetic Resonance Imaging. J. Phys. Chem. C. 2009; 113:20855–20860.
37. Caravan P, Ellison JJ, McMurry TJ, Lauffer RB. Gadolinium(III) Chelates as MRI Contrast Agents: Structure, Dynamics, and Applications. Chem. Rev. 1999; 99:2293–2352. [PubMed: 11749483]
38. Lauffer RB. Paramagnetic Metal-Complexes as Water Proton Relaxation Agents for Nmr Imaging - Theory and Design. Chem. Rev. 1987; 87:901–927.
39. Helm L. Relaxivity in Paramagnetic Systems: Theory and Mechanisms. Prog. Nucl. Magn. Reson. Spectrosc. 2006; 49:45–64.
40. Benetis N, Kowalewski J, Nordenskiold L, Wennerstrom H, Westlund PO. Nuclear-Spin Relaxation in Paramagnetic Systems - the Slow Motion Problem for Electron-Spin Relaxation. Mol. Phys. 1983; 48:329–346.
41. Larsson T, Westlund PO, Kowalewski J, Koenig SH. Nuclear-Spin Relaxation in Paramagnetic-Complexes in the Slow-Motion Regime for the Electron-Spin - the Anisotropic Pseudorotation Model for S=1 and the Interpretation of Nuclear Magnetic- Relaxation Dispersion Results for a Low-Symmetry Ni(Ii) Complex. J. Chem. Phys. 1994; 101:1116–1128.

42. Nilsson T, Kowalewski J. Slow-Motion Theory of Nuclear Spin Relaxation in Paramagnetic Low-Symmetry Complexes: A Generalization to High Electron Spin. J. Magn. Reson. 2000; 146:345–358. [PubMed: 11001850]
43. Rast S, Fries PH, Belorizky E, Borel A, Helm L, Merbach AE. A General Approach to the Electronic Spin Relaxation of Gd(III) Complexes in Solutions. Monte Carlo Simulations Beyond the Redfield Limit. J. Chem. Phys. 2001; 115:7554–7563.
44. Bonnet CS, Fries PH, Gadelle A, Gambarelli S, Delangle P. A Rigorous Framework to Interpret Water Relaxivity. The Case Study of a Gd(III) Complex with an Alpha-Cyclodextrin Derivative. J. Am. Chem. Soc. 2008; 130:10401–10413. [PubMed: 18620395]
45. Bertini I, Galas O, Luchinat C, Parigi G. Computer-Program for the Calculation of Paramagnetic Enhancements Nuclear-Relaxation Rates in Slowly Rotating Systems. J. Magn. Reson. A. 1995; 113:151–158.
46. Bertini I, Kowalewski J, Luchinat C, Nilsson T, Parigi G. Nuclear Spin Relaxation in Paramagnetic Complexes of S=1: Electron Spin Relaxation Effects. J. Chem. Phys. 1999; 111:5795–5807.
47. Kruk D, Nilsson T, Kowalewski J. Nuclear Spin Relaxation in Paramagnetic Systems with Zero-Field Splitting and Arbitrary Electron Spin. Phys. Chem. Chem. Phys. 2001; 3:4907–4917.
48. Song Y, Xu XY, MacRenaris KW, Zhang XQ, Mirkin CA, Meade TJ. Multimodal Gadolinium-Enriched DNA-Gold Nanoparticle Conjugates for Cellular Imaging. Angew. Chem. Int. Ed. 2009; 48:9143–9147.
49. Lee SM, Song Y, Hong BJ, MacRenaris KW, Mastarone DJ, O'Halloran TV, Meade TJ, Nguyen ST. Modular Polymer-Caged Nanobins as a Theranostic Platform with Enhanced Magnetic Resonance Relaxivity and pH-Responsive Drug Release. Angew. Chem. Int. Ed. 2010; 49:9960–9964.
50. Karfeld-Sulzer LS, Waters EA, Davis NE, Meade TJ, Barron AE. Multivalent Protein Polymer MRI Contrast Agents: Controlling Relaxivity Via Modulation of Amino Acid Sequence. Biomacromolecules. 2010; 11:1429–1436. [PubMed: 20420441]
51. Endres PJ, Paunesku T, Vogt S, Meade TJ, Woloschak GE. DNA-TiO2 Nanoconjugates Labeled with Magnetic Resonance Contrast Agents. J. Am. Chem. Soc. 2007; 129:15760–15761. [PubMed: 18047347]
52. Bull SR, Guler MO, Bras RE, Meade TJ, Stupp SI. Self-Assembled Peptide Amphiphile Nanofibers Conjugated to MRI Contrast Agents. Nano Lett. 2005; 5:1–4. [PubMed: 15792402]
53. Platas-Iglesias C, Vander Elst L, Zhou WZ, Muller RN, Geraldes CFGC, Maschmeyer T, Peters JA. Zeolite GdNaY Nanoparticles with Very High Relaxivity for Application as Contrast Agents in Magnetic Resonance Imaging. Chem. Eur. J. 2002; 8:5121–5131. [PubMed: 12613030]
54. Ali MM, Woods M, Caravan P, Opina ACL, Spiller M, Fettinger JC, Sherry AD. Synthesis and Relaxometric Studies of a Dendrimer-Based pH-Responsive MRI Contrast Agent. Chem. Eur. J. 2008; 14:7250–7258. [PubMed: 18601236]
55. Gianolio E, Giovenzana GB, Longo D, Longo I, Menegotto I, Aime S. Relaxometric and Modelling Studies of the Binding of a Lipophilic Gd-AAZTA Complex to Fatted and Defatted Human Serum Albumin. Chem. Eur. J. 2007; 13:5785–5797. [PubMed: 17407109]
56. Aime S, Frullano L, Crich SG. Compartmentalization of a Gadolinium Complex in the Apoferritin Cavity: A Route to Obtain High Relaxivity Contrast Agents for Magnetic Resonance Imaging. Angew. Chem. Int. Ed. 2002; 41:1017–1019.
57. Moriggi L, Cannizzo C, Dumas E, Mayer CR, Ulianov A, Helm L. Gold Nanoparticles Functionalized with Gadolinium Chelates as High-Relaxivity MRI Contrast Agents. J. Am. Chem. Soc. 2009; 131:10828–10829. [PubMed: 19722661]
58. Allen M, Bulte JWM, Liepold L, Basu G, Zywicke HA, Frank JA, Young M, Douglas T. Paramagnetic Viral Nanoparticles as Potential High-Relaxivity Magnetic Resonance Contrast Agents. Magn. Reson. Med. 2005; 54:807–812. [PubMed: 16155869]
59. Caravan P, Farrar CT, Frullano L, Uppal R. Influence of Molecular Parameters and Increasing Magnetic Field Strength on Relaxivity of Gadolinium- and Manganese-Based T1 Contrast Agents. Contrast Media Mol. Imaging. 2009; 4:89–100. [PubMed: 19177472]

60. Laus S, Sitharaman B, Toth E, Bolskar RD, Helm L, Wilson LJ, Merbach AE. Understanding Paramagnetic Relaxation Phenomena for Water-Soluble Gadofullerenes. J. Phys. Chem. C. 2007; 111:5633–5639.
61. Laus S, Sitharaman B, Toth V, Bolskar RD, Helm L, Asokan S, Wong MS, Wilson LJ, Merbach AE. Destroying Gadofullerene Aggregates by Salt Addition in Aqueous Solution of Gd@C60(OH)(X) and Gd@C60[C(COOH2)](10). J. Am. Chem. Soc. 2005; 127:9368–9369. [PubMed: 15984854]
62. Lu J, Mei WN, Gao Y, Zeng XC, Jing MW, Li GP, Sabirianov R, Gao ZX, You LP, Xu J, Yu DP, Ye HQ. Structural and Electronic Properties of Gd@C60: All-Electron Relativistic Total-Energy Study. Chem. Phys. Lett. 2006; 425:82–84.
63. Paratala BS, Jacobson BD, Kanakia S, Francis LD, Sitharaman B. Physicochemical Characterization, and Relaxometry Studies of Micro-Graphite Oxide, Graphene Nanoplatelets, and Nanoribbons. PLoS One. 2012:7.
64. Dreyer DR, Park S, Bielawski CW, Ruoff RS. The Chemistry of Graphene Oxide. Chem. Soc. Rev. 2010; 39:228–240. [PubMed: 20023850]
65. Polyakova EY, Rim KT, Eom D, Douglass K, Opila RL, Heinz TF, Teplyakov AV, Flynn GW. Scanning Tunneling Microscopy and X-Ray Photoelectron Spectroscopy Studies of Graphene Films Prepared by Sonication-Assisted Dispersion. ACS Nano. 2011; 5:6102–6108. [PubMed: 21726071]
66. Moriya T, Takahashi Y. Itinerant Electron Magnetism. Annu. Rev. Mater. Sci. 1984; 14:1–25.
67. Yazyev OV, Helm L. Defect-Induced Magnetism in Graphene. Phys. Rev. B. 2007; 75:125408.
68. Hernandez Y, Nicolosi V, Lotya M, Blighe FM, Sun ZY, De S, McGovern IT, Holland B, Byrne M, Gun'ko YK, Boland JJ, Niraj P, Duesberg G, Krishnamurthy S, Goodhue R, Hutchison J, Scardaci V, Ferrari AC, Coleman JN. High-Yield Production of Graphene by Liquid-Phase Exfoliation of Graphite. Nat. Nanotechnol. 2008; 3:563–568. [PubMed: 18772919]
69. Duch MC, Budinger GRS, Liang YT, Soberanes S, Urich D, Chiarella SE, Campochiaro LA, Gonzalez A, Chandel NS, Hersam MC, Mutlu GM. Minimizing Oxidation and Stable Nanoscale Dispersion Improves the Biocompatibility of Graphene in the Lung. Nano Lett. 2011; 11:5201–5207. [PubMed: 22023654]
70. Kovtyukhova NI, Ollivier PJ, Martin BR, Mallouk TE, Chizhik SA, Buzaneva EV, Gorchinskiy AD. Layer-by-Layer Assembly of Ultrathin Composite Films from Micron-Sized Graphite Oxide Sheets and Polycations. Chem. Mater. 1999; 11:771–778.
71. Liu Z, Robinson JT, Sun XM, Dai HJ. PEGylated Nanographene Oxide for Delivery of Water-Insoluble Cancer Drugs. J. Am. Chem. Soc. 2008; 130:10876–10877. [PubMed: 18661992]
72. Rourke JP, Pandey PA, Moore JJ, Bates M, Kinloch IA, Young RJ, Wilson NR. The Real Graphene Oxide Revealed: Stripping the Oxidative Debris from the Graphene-Like Sheets. Angew. Chem. Int. Ed. 2011; 50:3173–3177.
73. Fernandez-Merino MJ, Guardia L, Paredes JI, Villar-Rodil S, Solis-Fernandez P, Martinez-Alonso A, Tascon JMD. Vitamin C Is an Ideal Substitute for Hydrazine in the Reduction of Graphene Oxide Suspensions. J. Phys. Chem. C. 2010; 114:6426–6432.
74. Wang B, Luo B, Liang M, Wang A, Wang J, Fang Y, Chang Y, Zhi L. Chemical Amination of Graphene Oxides and Their Extraordinary Properties in the Detection of Lead Ions. Nanoscale. 2011; 3:5059–5066. [PubMed: 22041992]
75. Wang S, Chia PJ, Chua LL, Zhao LH, Png RQ, Sivaramakrishnan S, Zhou M, Goh RGS, Friend RH, Wee ATS, Ho PKH. Band-Like Transport in Surface-Functionalized Highly Solution-Processable Graphene Nanosheets. Adv. Mater. 2008; 20:3440–3446.
76. Bourlinos AB, Gournis D, Petridis D, Szabo T, Szeri A, Dekany I. Graphite Oxide: Chemical Reduction to Graphite and Surface Modification with Primary Aliphatic Amines and Amino Acids. Langmuir. 2003; 19:6050–6055.
77. Compton OC, Dikin DA, Putz KW, Brinson LC, Nguyen ST. Electrically Conductive"Alkylated" Graphene Paper Via Chemical Reduction of Amine-Functionalized Graphene Oxide Paper. Adv. Mater. 2010; 22:892–896. [PubMed: 20217812]

78. Djanashvili K, Peters JA. How to Determine the Number of Inner-Sphere Water Molecules in Lanthanide(III) Complexes by 17O NMR Spectroscopy. A Technical Note. Contrast Media Mol. Imaging. 2007; 2:67–71. [PubMed: 17451189]

79. Supkowski RM, Horrocks WD. On the Determination of the Number of Water Molecules, q, Coordinated to Europium(III) Ions in Solution from Luminescence Decay Lifetimes. Inorg. Chim. Acta. 2002; 340:44–48.

80. Kim J, Cote LJ, Kim F, Huang JX. Visualizing Graphene Based Sheets by Fluorescence Quenching Microscopy. J. Am. Chem. Soc. 2010; 132:260–267. [PubMed: 19961229]

81. Ashcroft, NW.; D, MN. Solid State Physics. Belmont, CA: Brooks Cole; 1976. p. 675

82. Aime S, Botta M, Fasano M, Paoletti S, Terreno E. Relaxometric Determination of the Exchange Rate of the Coordinated Water Protons in a Neutral Gd-III Chelate. Chem. Eur. J. 1997; 3:1499–1504.

83. de la Torre JG, Huertas ML, Carrasco B. Hydronmr: Prediction of NMR Relaxation of Globular Proteins from Atomic-Level Structures and Hydrodynamic Calculations. J. Magn. Reson. 2000; 147:138–146. [PubMed: 11042057]

84. Lipari G, Szabo A. Model-Free Approach to the Interpretation of Nuclear Magnetic-Resonance Relaxation in Macromolecules .1. Theory and Range of Validity. J. Am. Chem. Soc. 1982; 104:4546–4559.

85. Caravan P, Parigi G, Chasse JM, Cloutier NJ, Ellison JJ, Lauffer RB, Luchinat C, McDermid SA, Spiller M, McMurry TJ. Albumin Binding, Relaxivity, and Water Exchange Kinetics of the Diastereoisomers of MS-325, a Gadolinium(III)-Based Magnetic Resonance Angiography Contrast Agent. Inorg. Chem. 2007; 46:6632–6639. [PubMed: 17625839]

86. Torres S, Martins JA, Andre JP, Geraldes CFGC, Merbach AE, Toth E. Supramolecular Assembly of an Amphiphilic Gd-III Chelate: Tuning the Reorientational Correlation Time and the Water Exchange Rate. Chem. Eur. J. 2006; 12:940–948. [PubMed: 16224764]

87. Kowall T, Foglia F, Helm L, Merbach AE. Molecular-Dynamics Simulation Study of Lanthanide Ions Ln(3+) in Aqueous-Solution - Analysis of the Structure of the First Hydration Shell and of the Origin of Symmetry Fluctuations. J. Phys. Chem. 1995; 99:13078–13087.

88. Caravan P. Strategies for Increasing the Sensitivity of Gadolinium Based MRI Contrast Agents. Chem. Soc. Rev. 2006; 35:512–523. [PubMed: 16729145]

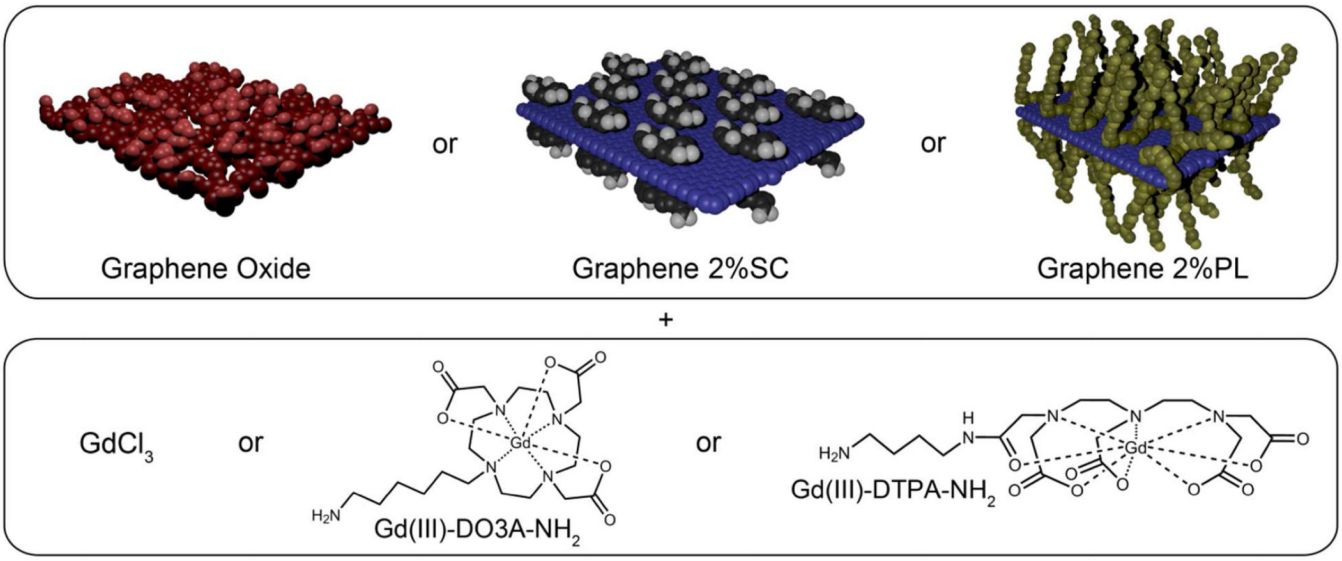


| | Gd(III) Graphene Oxide | Gd(III) Graphene 2%SC | Gd(III) Graphene 2%PL | Gd(III)-DTPA Graphene Oxide | Gd(III)-DO3A Graphene Oxide | Gd(III)-DO3A Graphene 2%SC | Gd(III)-DO3A Graphene 2%PL |
|---|---|---|---|---|---|---|---|
| $r_1$ | 78 - 85 | 46 - 59 | 20 - 30 | 28 - 32 | 49 - 63 | 25 | 12 - 17 |
| $r_2$ | 103 - 115 | 78 - 94 | 24 - 48 | 46 - 51 | 86 - 102 | 47 | 25 - 29 |
| Gd/C | 52 - 72 | 6 - 12 | 3 - 11 | 73 - 89 | 74 - 120 | 21 | 12 - 47 |

$r_1$ and $r_2$ are in $mM^{-1}s^{-1}$, measured at 60 MHz and 37°C, Gd/C is in Gd per 10,000 C

**Figure 1.**

Overview of gadographene materials prepared and investigated. Gadographenes have unusually large relaxivities that are comparable to other Gd(III)-carbon nanomaterials and greater than most nanomaterial or macromolecular agents based on Gd(III). SC = sodium cholate. PL = Pluronic F108NF. $r_1$ = longitudinal relaxivity. $r_2$ = transverse relaxivity.

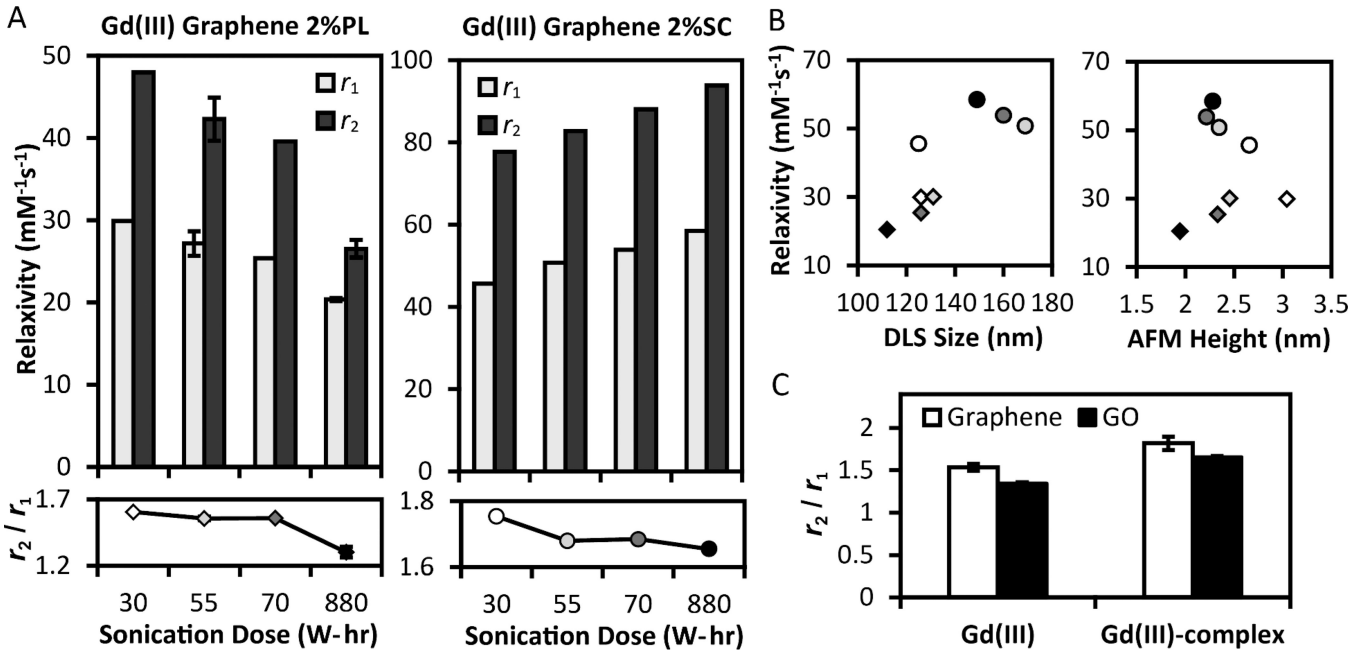


**Figure 2.**

(A) Relaxivity ($r_1$ and $r_2$) at 60 MHz as a function of sonication dose for Gd(III) Graphene 2%PL and 2%SC. The trend is opposite for the two surfactants. (B) Sonication results in thinner graphene stacks, as measured by DLS and AFM height, but no clear positive correlation between relaxivity and graphene size is detected. Symbols and shades in (B) indicate surfactant choice and sonication dose as in (A). More pristine gadographenes possess larger $r_2/r_1$ ratios than more damaged gadographenes (A) and materials based on graphene oxide (C) for both $GdCl_3$ and Gd(III)-complexes (Gd(III)-DO3A-$NH_2$ and Gd(III)-DTPA-$NH_2$). Where available, error bars represent standard error.

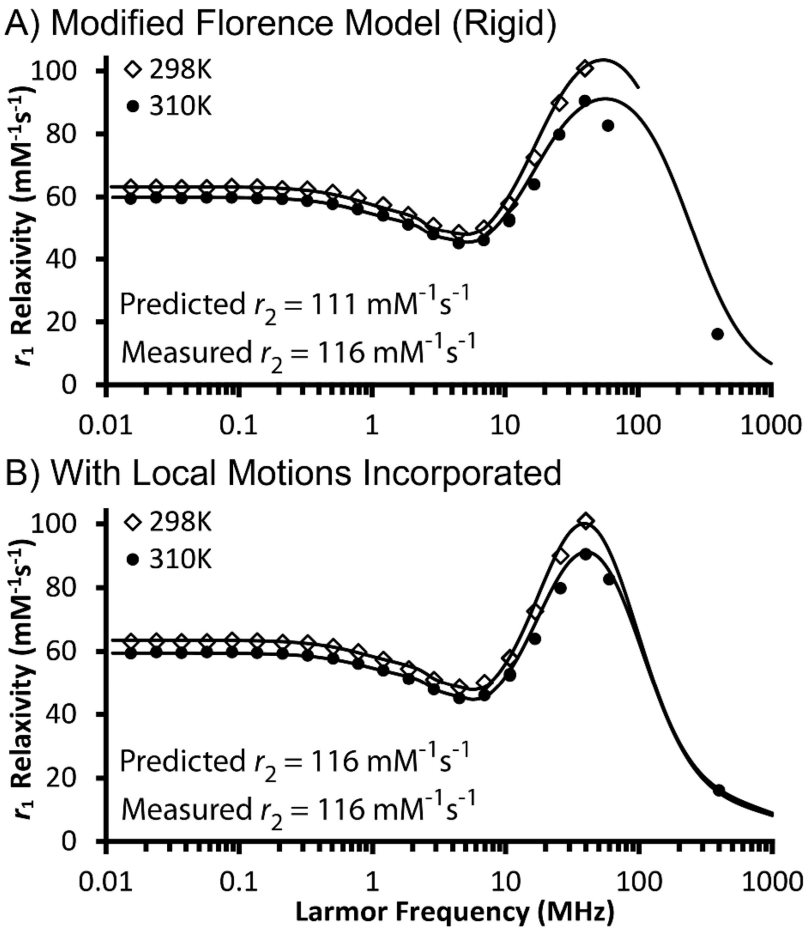


| Measured values | | Fitted values | | |
|---|---|---|---|---|
| $q$ | 5 | | Modified Florence 298K/310K | Lipari-Szabo 298K/310K |
| $\mu_{eff}$ ($\mu_B$) | 7.3 | | | |
| **Literature values**[37,82] | | $\tau_R$ (ns) | ≥ 1000 | ≥ 1000 |
| $r$ (Å) | 3.1 | $S^2$ | N/A | 0.43 |
| $d$ (Å) | 3.8 | $\tau_{fast}$ (ps) | N/A | 120/100 |
| $D_{diff}$ 298K | $2.3 \times 10^{-5}$ | $\tau_M$ (ns) | 0.74/0.64 | 1.8/1.6 |
| ($cm^2/s$) 310K | $3.3 \times 10^{-5}$ | $T_{1e}^{100kHz}$ (ps) | 176/181 | 197/206 |

**Figure 3.**

Mechanism of Gd(III) Graphene Oxide-induced proton relaxation. Gd(III) was found to experience local mobility based on analysis of the NMRD profiles at 298 and 310K; better fits were obtained when the modified Florence model (A) incorporated the Lipari-Szabo order parameter $S^2$ (B). The observed high relaxivity is derived from a $q$ of 5 and a $\tau_R \geq$ 1000 ns while fast local motions ($\tau_{fast}$ and $S^2$) and a $\tau_M < 10$ ns act as limiting factors. The fitted parameters accurately predicted the transverse relaxivity ($r_2$) measured at 60 MHz, 310K. $q$ = hydration number, $\mu_{eff}$ = effective magnetic moment, $\mu_B$ = Bohr magneton, $r$ = Gd(III)-proton distance, $d$ = distance of closest approach, $D_{diff}$ = diffusion coefficient, $\tau_R$ =

rotational correlation time, $S^2$ = order paramter, $\tau_{fast}$ = fast motion correlation time, $\tau_M$ = mean water residence time, $T_{1e}$ = longitudinal electronic relaxation time.

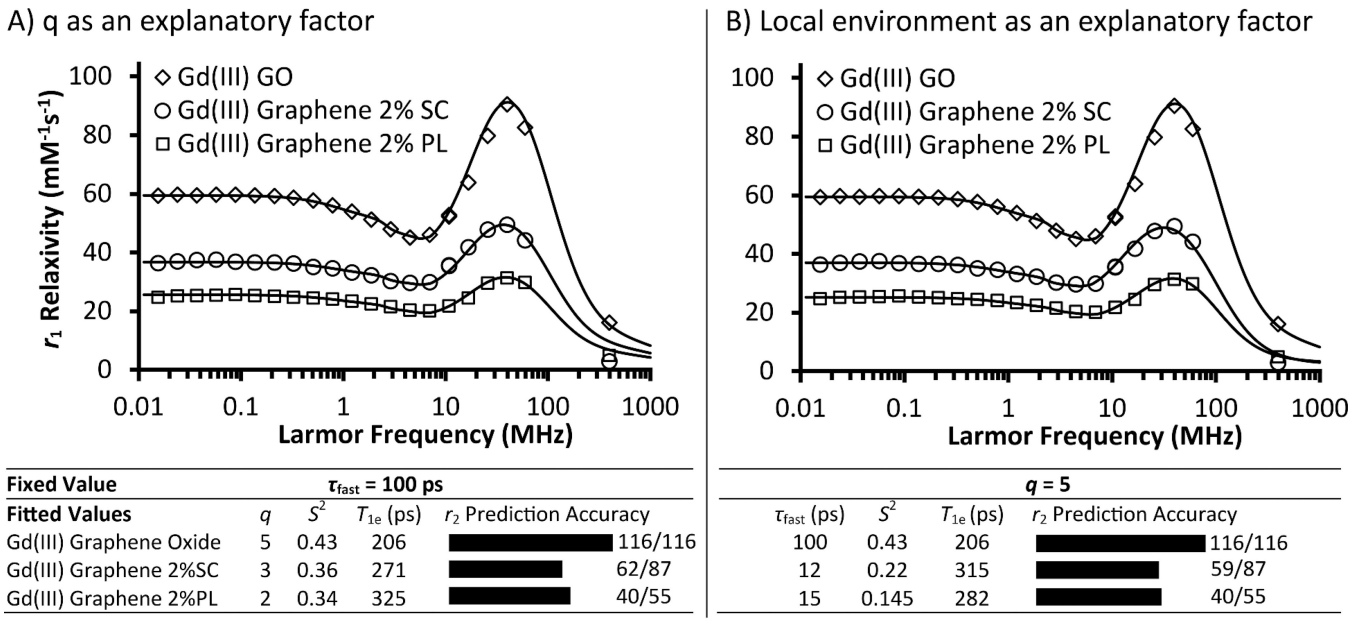


| Fixed Value | | $\tau_{fast}$ = 100 ps | | | |
|---|---|---|---|---|---|
| **Fitted Values** | $q$ | $S^2$ | $T_{1e}$ (ps) | $r_2$ Prediction Accuracy | |
| Gd(III) Graphene Oxide | 5 | 0.43 | 206 | | 116/116 |
| Gd(III) Graphene 2%SC | 3 | 0.36 | 271 | | 62/87 |
| Gd(III) Graphene 2%PL | 2 | 0.34 | 325 | | 40/55 |

| | $q$ = 5 | | | |
|---|---|---|---|---|
| $\tau_{fast}$ (ps) | $S^2$ | $T_{1e}$ (ps) | $r_2$ Prediction Accuracy | |
| 100 | 0.43 | 206 | | 116/116 |
| 12 | 0.22 | 315 | | 59/87 |
| 15 | 0.145 | 282 | | 40/55 |

In both analyses, fitting was performed by fixing $r$ = 3.1 Å, $d$ = 3.8 Å, $D_{diff} = 3.3 \times 10^{-5}$ cm$^2$/s, $\tau_R \geq 1000$ ns, $\tau_M$ = 1.6 ns
$r_2$ Prediction Accuracy is defined as $r_2$,predicted / $r_2$,measured, bars shown are relative; $T_{1e}$ is reported at 100 kHz

**Figure 4.**

Mechanism of Gd(III) Graphene-induced proton relaxation. Similar to Gd(III) GO, local motions were found to be an important feature of Gd(III) Graphene. Their NMRD profiles were analyzed by the modified Florence model incorporating the Lipari-Szabo approach. The relaxivity of Gd(III) Graphene depended on the choice of surfactant (SC or PL) and was reduced compared to Gd(III) GO. Possible explanations include 1) decreased $q$ by transient surfactant coordination to Gd(III), 2) a difference in Gd(III) microenvironments that resulted in different local motions and $S^2$, 3) reduced water access due to a surfactant-posed diffusion barrier, or some combination of the three factors. The plausibility of the first two explanations were supported by NMRD fitting in (A) and (B), respectively. Theory consistently underestimated the $r_2$ of Gd(III) Graphene, as shown by the $r_2$ prediction accuracy.

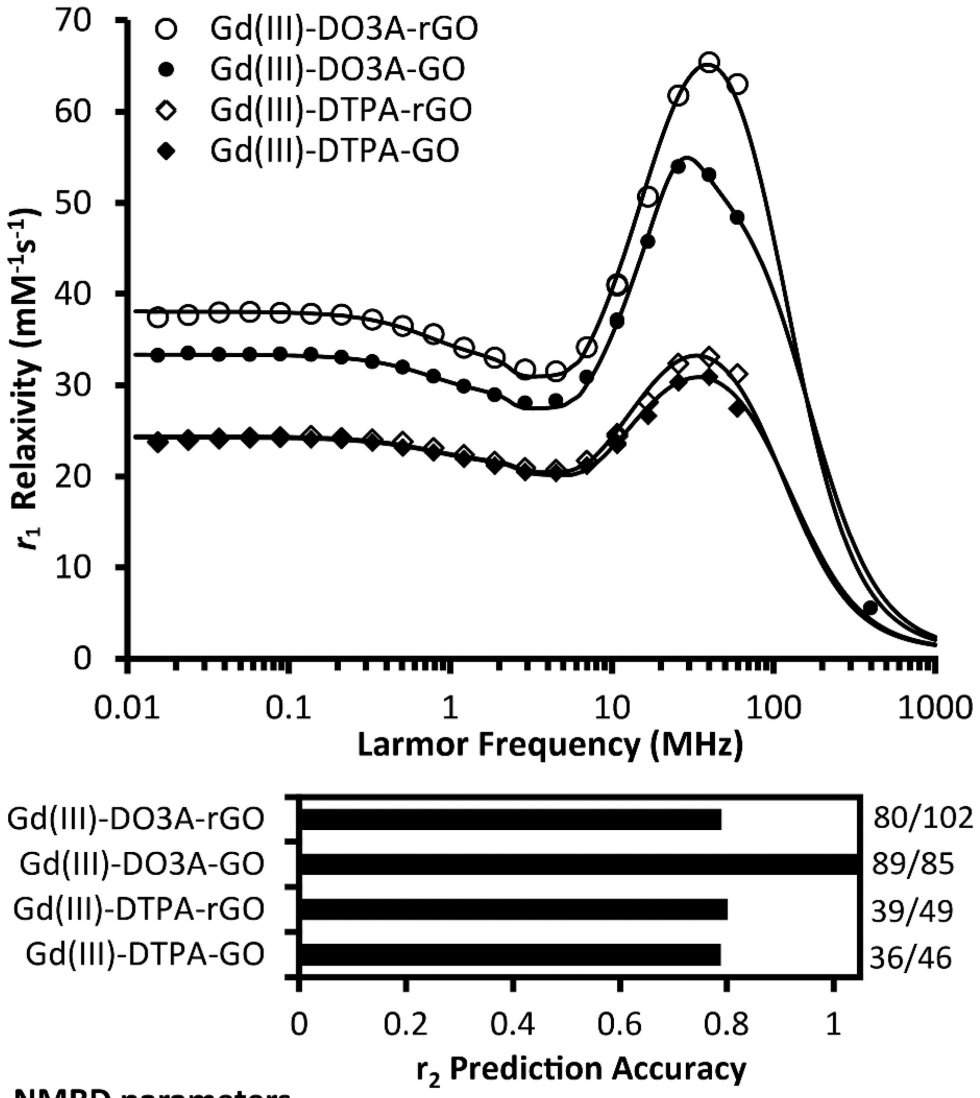


**NMRD parameters**

| | $S^2$ | $\tau_{fast}$ (ns) | $T_{1e}^{100kHz}$ (ps) | $\tau_M$ (ns) | $q$ |
|---|---|---|---|---|---|
| Gd(III)-DO3A-rGO | 0 | 1.55 | 381 | 77 | 2 |
| Gd(III)-DO3A-GO | .06 | 1.05 | 325 | 77 | 2 |
| Gd(III)-DTPA-rGO | 0 | 1.65 | 398 | 130 | 1 |
| Gd(III)-DTPA-GO | 0 | 1.44 | 398 | 130 | 1 |

**Figure 5.**

Mechanism of Gd(III)-Complex Graphene Oxide-induced proton relaxation. Gd(III)-DO3A-$NH_2$ ($q$=2) or Gd(III)-DTPA-$NH_2$ ($q$=1) was conjugated to either GO or reduced GO (rGO). Analysis of the NMRD profiles shows that these agents have higher relaxivities per $q$ compared to Gd(III) GO as a result of their more optimized $\tau_M$ and slower local motion. The near-zero values of $S^2$ suggest isotropic tumbling of Gd(III)-complexes on the GO surface. Consistent with the findings in Gd(III) Graphene, $r_2$ prediction ($r_{2,predicted}$ / $r_{2,measured}$ ) using the fitted parameters is more accurate for Gd(III)-DO3A-GO than for its rGO counterpart. $\tau_M$ and $q$ of the complexes were obtained from literature[37] and assumed to remain unchanged post-conjugation.